Matter-wave dark solitons and their excitation spectra in spin-orbit coupled Bose-Einstein condensates

V. Achilleos and D. J. Frantzeskakis
Department of Physics, University of Athens, Panepistimiopolis, Zografos, Athens 157 84, Greece

J. Stockhofe*
Zentrum für Optische Quantentechnologien, Universität Hamburg, Luruper Chaussee 149, 22761 Hamburg, Germany

P. G. Kevrekidis
Department of of Mathematics and Statistics, University of Massachusetts, Amherst, MA 01003-9305, USA

P. Schmelcher
Zentrum für Optische Quantentechnologien, Universität Hamburg, Luruper Chaussee 149, 22761 Hamburg, Germany and The Hamburg Centre for Ultrafast Imaging, Luruper Chaussee 149, 22761 Hamburg, Germany

We present three types of dark solitons in quasi-one-dimensional spin-orbit coupled repulsive Bose-Einstein condensates. Among these families, two are always stable, while the third one is only stable sufficiently close to the linear regime. The solitons' excitation spectra reveal the potential existence of a *second* anomalous mode. While the first such mode describes the soliton oscillatory motion in a parabolic trap, the second, when present, reflects the double well structure of the underlying single-particle spectrum. This novel mode results in moving density stripes in the vicinity of the soliton core, or in an out-of-phase oscillation of the constituent components, with little effect on the nearly stationary striped total density of the composite soliton.

INTRODUCTION

The recent experimental realization of spin-orbit coupling (SOC) in Bose-Einstein condensates (BECs) [1–3] and fermionic gases [4, 5] has stimulated considerable research interest. This is due to the fact that it paves the way towards a deeper understanding of exotic solid state systems such as topological insulators, making use of the highly controllable environment of cold atom physics [6, 7]. Ultracold atomic gases promise to be an ideal system for the generation of versatile artificial gauge fields [8] and studying such Abelian or even non-Abelian gauge fields is relevant not only in mimicking solid state physics, but potentially even to fundamental theories such as quantum electro- or chromodynamics [9].

In the above context, ground state properties of SOC-BECs, including phase separation and the existence of the stripe phase [10], as well as the collective dynamics and oscillations [11], have already been studied in some detail both in theory and experiments [1, 2]. Furthermore, a relevant direction that has also attracted much attention is the study of topological excitations, such as skyrmions [12], vortices [13], and Dirac monopoles [14]; additionally, dark solitons in toroidal geometry [15] and bright solitons in quasi one-dimensional (1D) attractive SOC-BECs [16] have also been predicted. While the above structures have already been studied extensively in the context of single- and multi-component BECs [17, 18], the presence of SOC can significantly enrich their structural, stability and dynamical properties.

It is the purpose of this work to highlight the above by presenting and analyzing dark soliton states in SOC-BECs confined in a highly anisotropic (quasi-1D) parabolic trap. Employing a multiscale expansion method, we find three different dark soliton families, featuring either a constant or a spatially modulated background density; in the latter case, dark solitons occur as excited states on top of the stripe phase of SOC-BECs (we call these states "stripe solitons"). We perform a Bogolyubov-de Gennes (BdG) linearization analysis of the above soliton families, showing that constant background solitons are always stable, while stripe solitons are stable only close to the linear limit. The characteristic negative energy (anomalous) mode associated with the oscillation frequency of solitons near the trap center is identified within the excitation spectrum and its eigenfrequency is determined analytically. Importantly, in certain parameter regions we also find a *second* anomalous mode, which does not exist in single- or multi-component BECs, and is only sustained due to the double well structure of the SOC single particle spectrum, featuring two minima. Exciting this mode, we observe intriguing dynamics: constant background solitons feature moving stripes in the vicinity of the soliton core, somewhat reminiscent of the Kelvin mode modulation of vortex lines [19]; on the other hand, in the case of stripe solitons, we observe an out-of-phase oscillation of the constituent solitons, which does not affect the stationary total density of the composite state.

THE MODEL AND ITS ANALYTICAL CONSIDERATION

We consider a SOC-BEC confined in a quasi-1D parabolic trap, with longitudinal and transverse frequencies $\omega_x \ll \omega_\perp$. In the framework of mean-field theory, this system can be described by the energy functional [1, 10]:

$$\mathcal{E} = \mathbf{u}^\dagger \mathcal{H}_0 \mathbf{u} + \frac{1}{2}\left(g_{11}|u|^4 + g_{22}|v|^4 + 2g_{12}|u|^2|v|^2\right), \tag{1}$$

where $\mathbf{u} \equiv (u, v)^T$, and the condensate wavefunctions u and v are related (through suitable rotations [1]) to the two pseudo-spin components of the BEC. The single particle Hamiltonian $\mathcal{H}_0$ in Eq. (1) reads: $\mathcal{H}_0 = \frac{1}{2m}(\hat{p}_x \mathbb{1} + k_L \hat{\sigma}_z)^2 + V_{\rm tr}(x)\mathbb{1} + \Omega\hat{\sigma}_x + \delta\hat{\sigma}_z$, where $\hat{p}_x = -i\hbar\partial_x$ is the momentum operator in the longitudinal direction, m is the atomic mass, $\hat{\sigma}_{x,z}$ are the Pauli matrices, $\mathbb{1}$ is the unit matrix, k_L is the wavenumber of the Raman laser which couples the states u and v, δ is the detuning from Raman resonance, and Ω is the strength of the Raman coupling. Additionally, $V_{\rm tr}(x)$ is the external trapping potential, considered to assume the usual parabolic form: $V_{\rm tr} = (1/2)m\omega_x^2 x^2$. Finally, the effectively 1D coupling constants g_{ij}, are given by $g_{ij} = 2\hbar\omega_\perp \alpha_{ij}$, where α_{ij} are the s-wave scattering lengths (assumed to be positive). Measuring energy in units of $\hbar\omega_\perp$, length in units of the transverse harmonic oscillator length $a_\perp = \sqrt{\hbar/(m\omega_\perp)}$, time in units of $\omega_\perp^{-1}$, and densities in units of the scattering length α_{11}, we derive from Eq. (1) the following dimensionless equations of motion:

$$\begin{aligned} i\partial_t u &= \left(-\frac{1}{2}\partial_x^2 - ik_L\partial_x + V_{\rm tr} + |u|^2 + \beta|v|^2 + \delta\right)u + \Omega v, \\ i\partial_t v &= \left(-\frac{1}{2}\partial_x^2 + ik_L\partial_x + V_{\rm tr} + \beta|u|^2 + \gamma|v|^2 - \delta\right)v + \Omega u, \end{aligned} \tag{2}$$

where $\beta = \alpha_{12}/\alpha_{11}$, $\gamma = \alpha_{22}/\alpha_{11}$, and we have used $k_L \to k_L/a_\perp$, $\Omega \to \Omega\hbar\omega_\perp$ and $\delta \to \delta\hbar\omega_\perp$; the trapping potential in Eqs. (2) is now given by $V_{\rm tr}(x) = (1/2)\omega_{\rm tr}^2 x^2$, where $\omega_{\rm tr} \equiv \omega_x/\omega_\perp$. The stationary counterpart of Eqs. (2) is obtained by factorizing $\mathbf{u}(x,t) = \mathbf{u}(x)\exp(-i\mu t)$, where μ denotes the chemical potential.

In the following, we adopt experimentally relevant values for the above parameters. Considering, as in the case of the experiments of Ref. [1], two spin states of the ^{87}Rb $5S_{1/2}$, $F = 1$ manifold, we will use the following dimensionless parameter values: Raman wavenumber $k_L = 8$, normalized Raman coupling strength $\Omega \in [0, 100]$, and ratios of the scattering lengths $\alpha_{11} : \alpha_{12} : \alpha_{22} = 1 : 0.995 : 0.995$. It is thus physically relevant to use below the approximation $\gamma \approx 1$ while we will let β be a free parameter.

We now use a multiscale perturbation method to derive approximate dark soliton solutions of Eqs. (2). First we introduce the ansatz: $\mathbf{u} = [U, V]^T \exp[i(kx - \mu t)]$, where k is the momentum and $\mu = \omega + \epsilon^2\omega_0$ the chemical potential, where ω is the energy in the linear limit, $\epsilon^2\omega_0$ is a small deviation about this energy ($0 < \epsilon \ll 1$), and $\omega_0/\omega = \mathcal{O}(1)$. We also assume that the trap strength is $\omega_{\rm tr} = \epsilon^2\tilde{\omega}_{\rm tr}$. Next, introducing the slow variables $T = \epsilon^2 t$, $X = \epsilon x$, and expanding U and V as $U = \epsilon U_1(X,T) + \epsilon^2 U_2(X,T) + \ldots$ and $V = \epsilon V_1(X,T) + \epsilon^2 V_2(X,T) + \ldots$, we derive from Eqs. (2) the following equations at the orders $\mathcal{O}(\epsilon^1)$, $\mathcal{O}(\epsilon^2)$ and $\mathcal{O}(\epsilon^3)$, respectively:

$$\mathbf{W}\mathbf{u}_1 = 0, \tag{3}$$

$$\mathbf{W}\mathbf{u}_2 = i\mathbf{W_0}\partial_X \mathbf{u}_1, \tag{4}$$

$$\mathbf{W}\mathbf{u}_3 = i\mathbf{W_0}\partial_X \mathbf{u}_2 - \left(i\partial_T + \frac{1}{2}\partial_X^2 - \mathbf{A} + \omega_0\right)\mathbf{u}_1, \tag{5}$$

where $\mathbf{u}_i = [U_i, V_i]^T$ ($i \in \{1, 2, 3\}$) are unknown vectors, and matrices $\mathbf{W}$ and $\mathbf{A}$ are given by:

$$\mathbf{W} = \begin{bmatrix} \omega - k^2/2 - kk_L - \delta & -\Omega \\ -\Omega & \omega - k^2/2 + kk_L + \delta \end{bmatrix},$$

$$\mathbf{A} = \begin{bmatrix} |U_1|^2 + \beta|V_1|^2 + \tilde{V}_{\rm tr} & 0 \\ 0 & \beta|U_1|^2 + |V_1|^2 + \tilde{V}_{\rm tr} \end{bmatrix},$$

where $\mathbf{W_0} = (\mathbf{W} - \omega\mathbb{1})'$, primes denote differentiation with respect to k, and $\tilde{V}_{\rm tr}(X) = (1/2)\tilde{\omega}_{\rm tr}^2 X^2$. At $\mathcal{O}(\epsilon^1)$, the solvability condition $\det\mathbf{W} = 0$ yields the single-particle spectrum (dispersion relation)

$$\omega = \omega_\pm(k) = \frac{1}{2}k^2 \pm \sqrt{(kk_L + \delta)^2 + \Omega^2}, \tag{6}$$

displayed in Fig 1. Let $\mathbf{L} = [1, Q]$ and $\mathbf{R} = [1, Q]^T$ be the left and right eigenvectors of $\mathbf{W}$ at eigenvalue 0, where

$$Q = Q(\omega, k) \equiv \frac{1}{\Omega}\left(\omega - \frac{1}{2}k^2 - kk_L - \delta\right). \tag{7}$$

Then, the compatibility condition of Eq. (3) yields:

$$\mathbf{u}_1 = \mathbf{R}\psi(X,T), \tag{8}$$

where $\psi(X,T)$ is an unknown scalar field.

Next, proceeding with Eq. (4), the compatibility condition $\mathbf{L}\mathbf{W_0}\mathbf{R} = 0$ at the order $\mathcal{O}(\epsilon^2)$ enforces a vanishing group velocity $v_g \equiv \partial\omega/\partial k$, *i.e.*:

$$v_g = k - k_L\frac{Q^2 - 1}{Q^2 + 1} = 0. \tag{9}$$

Thus, the compatibility condition at $\mathcal{O}(\epsilon^2)$ requires that the parameters ω and k are evaluated at stationary points of the dispersion relation (6). In the following we focus on the energy *minima* $(\omega_{\rm min}, k_{\rm min})$. Additionally, at the order $\mathcal{O}(\epsilon^2)$, we obtain the following solution for $\mathbf{u}_2$:

$$\mathbf{u}_2 = -i\mathbf{R}'\partial_X\psi(X,T). \tag{10}$$

Finally, at $\mathcal{O}(\epsilon^3)$, the compatibility condition for Eq. (5), combined with Eqs. (8) and the above result for $\mathbf{u}_2$, yields the following nonlinear Schrödinger (NLS) equation for the scalar field ψ:

$$i\partial_T\psi + \frac{\lambda}{2}\partial_X^2\psi - (\nu|\psi|^2 - \omega_0)\psi = \tilde{V}_{\rm tr}(X)\psi, \tag{11}$$

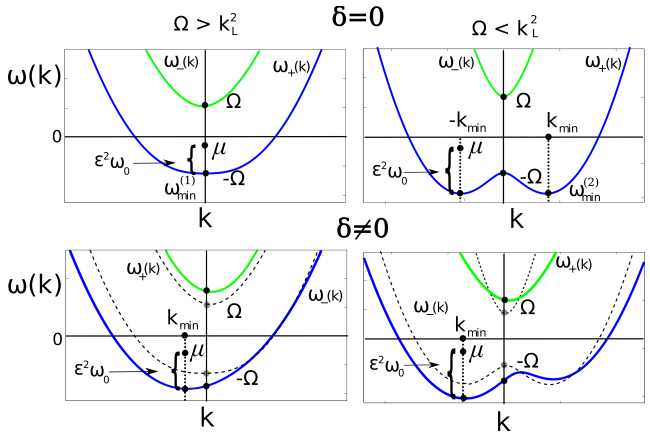

FIG. 1. (Color online) Sketches of the linear energy spectrum $\omega = \omega_{\pm}(k)$ for $\delta = 0$ (top panels) and $\delta \neq 0$ (bottom panels), and also for for $\Omega > k_L^2$ (left panels) and for $\Omega < k_L^2$ (right panels). In the bottom panels, dashed lines depict – for comparison – the respective curves corresponding to $\delta = 0$.

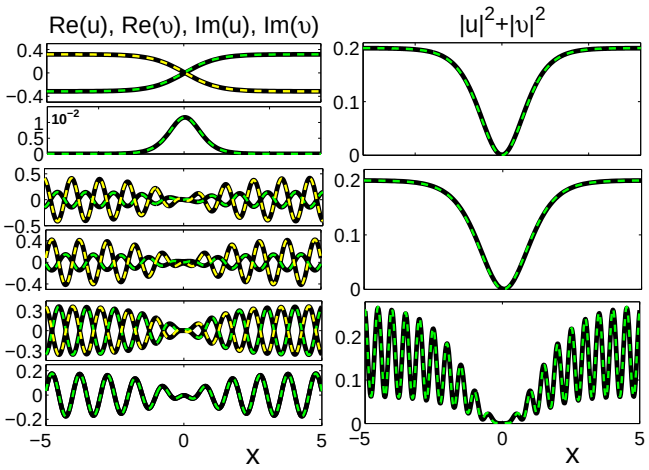

FIG. 2. (Color online) In each of the three triplets of panels, shown are the real (top left) and imaginary (bottom left) parts of u and v, as well as total density profiles $|u|^2 + |v|^2$ (right) of stationary kinks for $\delta = 0$, $\beta = 1$ and $\epsilon^2\omega_0 = 0.2$. The top triplet shows a soliton in Regime I for $\Omega/k_L^2 = 1.4$, while the middle and bottom triplets show a $k_{\rm min}$-soliton and a stripe soliton in Regime II for $\Omega/k_L^2 = 0.625$. Solid (black) lines depict numerical results, while dashed (green and yellow) lines correspond to analytical results [cf. Eqs. (13) and (15)].

where the coefficients λ and ν defined as:

$$\lambda = 1 - \frac{2QQ'(k_L - k)}{1 + Q^2}, \quad \nu = \frac{Q^4 + 2\beta Q^2 + 1}{1 + Q^2}, \tag{12}$$

are evaluated at the minima $(\omega, k) = (\omega_{\rm min}, k_{\rm min})$ of the dispersion relation (6).

In the homogeneous case ($\tilde{\omega}_{\rm tr} = 0$), for $\lambda\nu > 0$, and assuming the boundary conditions $|\psi|^2 \to \omega_0/\nu$ as $|X| \to \infty$, the above scalar NLS Eq. (11) possesses dark soliton solutions, $\psi_{\rm DS}$, characterized by the free parameter ω_0. A single dark soliton reads:

$$\psi_{\rm DS} = \sqrt{\omega_0/\nu}\,[\cos\theta \tanh(\eta) + i \sin\theta]\,, \tag{13}$$

where $\eta = \sqrt{\omega_0/\lambda}\cos\theta[X - X_0(T)]$, and θ is the so-called "soliton phase angle" controlling the velocity and the phase shift across the dark soliton ($|\theta| < \pi/2$). Additionally, $X_0(T)$ is the soliton center, while the soliton amplitude (depth) and soliton velocity are respectively given by $\sqrt{\omega_0/\lambda}\cos\theta$ and $\dot{X}_0 = \sqrt{\omega_0/\lambda}\sin\theta$. Note that the limiting case $\theta = 0$ corresponds to a stationary kink ("black" soliton), while cases with $\theta \neq 0$ give rise to traveling ("grey") solitons.

Using the above expressions, we can now write down an approximate dark soliton solution of Eqs. (2), in terms of

the original variables x and t, as follows:

$$\begin{pmatrix} u \\ v \end{pmatrix} \approx \epsilon \psi_{\rm DS} \exp\left[ik_{\rm min}x - i(\omega_{\rm min} + \epsilon^2\omega_0)t\right] \begin{pmatrix} 1 \\ Q_{\rm min} \end{pmatrix}, \tag{14}$$

where $\psi_{\rm DS}$ is given in Eq. (13), but with argument $\eta \to \eta/\epsilon$, and $Q_{\rm min} \equiv Q(\omega_{\rm min}, k_{\rm min})$.

DARK SOLITONS IN THE HOMOGENEOUS SETTING

The coefficients of the NLS equation (11) and thus the soliton parameters, explicitly depend on $Q_{\rm min}$, which is calculated at the minimum of the dispersion relation (6). The latter possesses an upper branch ω_+ and a lower branch ω_-, as shown in Fig. 1. We hereafter focus our analysis around the energy minima of the lower branch ω_-. We will study separately the regimes $\Omega/k_L^2 > 1$ (Regime I) and $\Omega/k_L^2 < 1$ (Regime II), for both $\delta = 0$ and $\delta \neq 0$, which feature different characteristics regarding the energy minima, as shown in the left and right panels of Fig. 1, respectively.

Dark solitons in Regime I. In this regime, and for $\delta = 0$, the lower branch possesses a minimum $\omega_{\rm min}^{(1)} = -\Omega$ at zero momentum $k_{\rm min} = 0$, while $Q_{\rm min} = -1$ and $Q'_{\rm min} = -k_L/\Omega$. The above values determine λ and ν in Eqs. (12) and, thus, the form of the soliton in Eq. (13). The existence of the relevant soliton solutions is numerically confirmed by solving the stationary version of Eqs. (2), where $\mu = -\Omega + \epsilon^2\omega_0$ [as per Eq. (13)], using a fixed-point algorithm [20]. A typical example of a stationary kink ($\theta = 0$), corresponding to parameter values $\Omega/k_L^2 = 1.4$ and $\epsilon^2\omega_0 = 0.2$, is shown in the top triplet of panels of Fig. 2. It is observed that the real parts of u and v (top left panel of the triplet) are opposite, in accordance with the form of the right eigenvector $\mathbf{R} = [1, -1]^T$; the imaginary parts (bottom left panel of the triplet) are of order $\mathcal{O}(\epsilon^2)$, and are equal having a sech^2 profile, in accordance to the analytical prediction for $\mathbf{u}_2$. Finally, the spatial profile of the total density $|u|^2 + |v|^2$ (top right panel) has the form of a scalar dark soliton's density [18].

Dark solitons in Regime II. In this regime, and for $\delta = 0$, we find solitons with energies near the energy minimum $\omega_{\rm min}^{(2)}$ at finite momenta, namely $k_{\rm min} = \pm k_L(1 - \Omega^2/k_L^4)^{1/2}$ (cf. top right panel of Fig. 1). For these values of the energy and momentum, $Q_{\rm min}^{(\pm)} = -k_{\rm min}\Omega^{-1}(k_L \pm k_{\rm min})$ and $Q_{\rm min}^{\prime(\pm)} = -\Omega^{-1}(k_L \pm k_{\rm min})$, with these values determining the soliton parameters in Eq. (12).

It is thus clear that, in this regime, two different soliton solutions can be found, each corresponding to the locations $k = \pm k_{\rm min}$ of the energy minimum; these will be called hereafter $\pm k_{\rm min}$-solitons. An example of a $k_{\rm min}$-soliton, for $\Omega/k_L^2 = 0.625$ and $\epsilon^2\omega_0 = 0.2$, is shown in the middle triplet of panels of Fig. 2. As can be seen, the real and imaginary parts of u and v have different amplitudes in this case, due to the form of $\mathbf{R} = [1, Q_{\rm min}^{(\pm)}]^T$; furthermore, Re$(u, v)$ and Im(u, v) are now spatially oscillatory with a wavelength $2\pi/k_{\rm min}$. On the other hand, the total density profile features the usual (*i.e.*, unmodulated) density dip.

Importantly, still another branch of dark soliton solutions can also be found in Regime II as follows. First we note that the respective linear problem in this regime admits solutions which are linear combinations of plane waves of momenta $k = \pm k_{\rm min}$. Then, employing continuation arguments, we construct approximate dark soliton solutions in the form of a linear combination of the above mentioned $\pm k_{\rm min}$-solitons. Solutions satisfying the symmetry $u = -\bar{v}$ (bar denotes complex conjugation) can be expressed as:

$$\begin{pmatrix} u \\ v \end{pmatrix} \approx \epsilon C \psi_{\rm DS} \begin{pmatrix} q_+ \cos(k_{\rm min}x) + iq_- \sin(k_{\rm min}x) \\ -q_+ \cos(k_{\rm min}x) + iq_- \sin(k_{\rm min}x) \end{pmatrix}, \tag{15}$$

where $q_\pm = \Omega^{-1} + Q_{\rm min}^{(\pm)}$ and C is a free parameter. The existence of these solitons was also confirmed numerically, and a pertinent example is shown in the bottom triplet of panels of Fig. 2, for $\Omega/k_L^2 = 0.625$, $\epsilon^2\omega_0 = 0.2$ and $C = 0.8$. It is observed that the soliton background features a spatially modulated density, reminiscent of the stripe phase of the SO-coupled BECs [10]; for this reason, solitons of this branch will be called "stripe solitons".

For all types of solitons found in Regimes I and II, the analytical approximations of Eqs. (13) and (15) are in an *excellent* agreement with the numerically obtained solutions (see, respectively, dashed and solid lines in Fig. 2). Furthermore, apart from the case of stationary (black) solitons, we have also studied traveling (grey) solitons with $\theta \neq 0$; this was done by direct numerical integration of Eqs. (2), by means of a Runge-Kutta method, using as initial conditions the analytical form of moving solitons, cf. Eq. (13). We have confirmed that near the linear limit (*i.e.*, for $\epsilon^2\omega_0 \lesssim 0.1$) the solitons remain robust and evolve without distortion (results not shown here).

The case of nonzero detuning parameter. Dark solitons can also be found for $\delta \neq 0$, upon calculating the energy minimum $(k_{\rm min}, \omega_{\rm min})$ of the lower branch of the energy spectrum (6) (cf. bottom panels of Fig. 1) and then using Eqs. (12) to determine the soliton parameters for the solution (13). There are two important differences between the

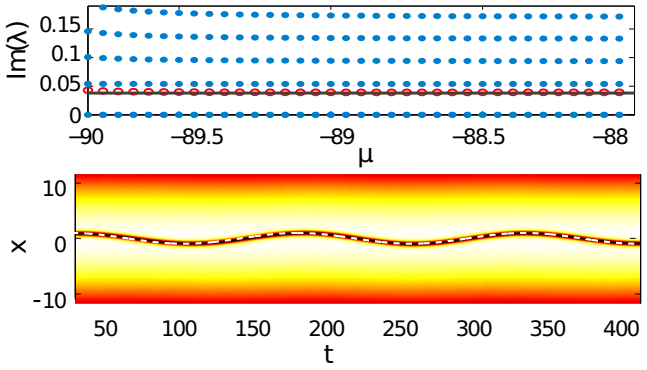

FIG. 3. (Color online) Top panel: the lowest imaginary eigenvalues of the linearization spectrum as functions of μ, for a dark soliton in Regime I, with $\delta = 0$, $\Omega/k_L^2 = 1.4$, and $\tilde{\omega}_{\rm tr} = 0.1$. Circles (in red) denote the anomalous mode eigenfrequency and the solid (black) line depicts the prediction of Eq. (16). Bottom panel: contour plot showing the evolution of the density of a SOC-BEC carrying a dark soliton initially placed at $x_0 = 1$. Dashed (white) line depicts the analytical result of Eq. (16).

cases $\delta \neq 0$ and $\delta = 0$. First, since $k_{\rm min} \neq 0$ for every $\delta \neq 0$ (see Fig. 1), the dark solitons in Regime I are shifted to finite k. Second, since in Regime II the degeneracy of the energy minima in the lower branch is always lifted for $\delta \neq 0$, stripe solitons cannot be constructed using the linear superposition argument as in Eq. (15). In both regimes, we have numerically confirmed the existence of dark solitons for $\delta \neq 0$ at the global minimum of the energy spectrum. As a result, in both regimes I and II, these structures share similar profiles to the ones presented in the middle triplet of panels of Fig. 2, hence they will not be shown here.

STABILITY AND DYNAMICS OF SOLITONS IN THE TRAP

We now focus on the experimentally relevant setting where the parabolic trap is present ($\tilde{\omega}_{\rm tr} \neq 0$). In this case, we have confirmed that all families of soliton solutions presented above persist. Furthermore, for the stationary solutions, we have performed a linear stability analysis and identified regimes of (in)stability. Our analysis relies on the study of the BdG excitation spectrum around a stationary soliton solution $\mathbf{u}_{\rm sol} \equiv (u_{\rm sol}, v_{\rm sol})^T$ of Eqs. (2), evolving at the chemical potential μ. The spectrum is obtained as follows. We introduce the ansatz $\mathbf{u} = \left\{\mathbf{u}_{\rm sol} + \varepsilon[\exp(\lambda t)\mathbf{a}(x) + \exp(\bar{\lambda} t)\bar{\mathbf{b}}(x)]\right\}\exp(-i\mu t)$, where ε is a formal small parameter, and $\{\lambda, (\mathbf{a}, \mathbf{b})\}$ define an eigenvalue-eigenvector pair. Then, substituting the above ansatz into Eqs. (2) and linearizing, we arrive at $\mathcal{O}(\varepsilon)$ at the ensuing eigenvalue problem for eigenvectors $(\mathbf{a}, \mathbf{b})$ and eigenvalues λ. Notice that as the latter are generally complex, *i.e.*, $\lambda = \lambda_r + i\lambda_i$, instability corresponds to $\lambda_r > 0$.

First, we consider the case of solitons in Regime I, for $\delta = 0$, and study their stability starting from the linear limit, $\mu = -\Omega$, and entering into the nonlinear regime by increasing the parameter ω_0. In the spectrum of the respective soliton branch, no real eigenvalues appear and, thus, this branch is dynamically stable. As shown in the top panel of Fig. 3 for $\Omega/k_L^2 = 1.4$ and $\omega_{\rm tr} = 0.1$, there exists one anomalous (negative energy) mode, depicted by red circles, whose frequency characterizes the small-amplitude oscillations of the dark soliton around the trap center. The latter can be obtained analytically in the framework of Eq. (11) as follows. As is well known, sufficiently deep (almost black) dark solitons oscillate in a parabolic trap of strength $\omega_{\rm tr}$ with a frequency $\omega_{\rm sol} = \omega_{\rm tr}/\sqrt{2}$ [18]. Hence, we can infer that solitons of Eq. (11) with $\theta \approx 0$ evolve in the trap so that their center $X_0(t)$ satisfies the equation of motion:

$$\frac{d^2 X_0}{dt^2} = -\frac{1}{2}\omega_{\rm sol}^2 X_0, \quad \omega_{\rm sol} = \sqrt{\frac{\lambda}{2}}\omega_{\rm tr}. \tag{16}$$

The above soliton oscillation frequency $\omega_{\rm sol}$ is depicted by the solid (black) line in the top panel of Fig. 3. It can be observed that this analytical result almost coincides with the anomalous mode eigenfrequency. To further elaborate on this result, we have numerically integrated Eqs. (2) with an initial condition of a soliton with $\theta = 0$, initially placed at $x_0 = 1$. As seen in the bottom panel of Fig. 3, the soliton indeed performs harmonic oscillations accurately described by Eq. (16), cf. dashed (white) line in the figure. We note that, for $\delta \neq 0$, solitons have a spectrum qualitatively similar to the one in Fig. 3, featuring one anomalous mode and no real (*i.e.*, unstable) eigenvalues.

Next, we study the stability of solitons in Regime II (for $\delta = 0$), in the presence of the trap. First we note that $k_{\rm min}$-solitons are stable, as no real eigenvalues appear in the spectrum – see the example shown in the top panel of

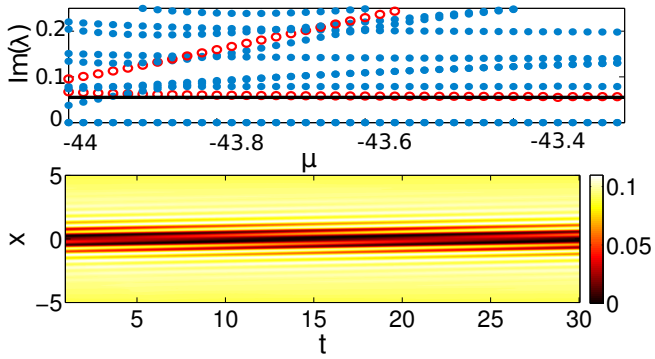

FIG. 4. (Color online) Top panel: same as the top panel of Fig. 3, but for the $k_{\rm min}$-solitons in Regime II with $\Omega/k_L^2 = 0.625$. Bottom panel: contour plot showing the evolution of the density of the u-component, when perturbed by the eigenvectors of the second anomalous mode at $\mu = -43.5$. Other parameter values are the same as in Fig. 3.

Fig. 4 for a soliton with $\Omega/k_L^2 = 0.625$. However, an important difference arises in this case, namely the emergence of a *second* anomalous mode in the linearization spectrum. Indeed, as shown in the figure [cf. circles (in red)], there exist two anomalous modes: a lower-lying one (with smaller eigenfrequencies), associated with the soliton oscillations as before, and an upper-lying anomalous mode (with larger eigenfrequencies). This second anomalous mode does not exist in the case of dark solitons in single- or multi-component BECs: its emergence is particular to dark solitons in SOC-BECs, which feature a double well structure in their energy spectrum in Regime II. Indeed, in the linear limit, the system possesses two eigenstates that energetically lie below the $k_{\rm min}$-soliton, namely one ground state configuration in each of the two wells of the energy spectrum. Each of these gives rise to one anomalous mode in the soliton's linearization spectrum. Superimposing the $k_{\rm min}$-soliton at momentum $k_{\rm min} > 0$ with the ground state at $k_{\rm min} > 0$ leads to the familiar soliton oscillation, represented by the lower-lying anomalous mode. On the other hand, superimposing the $k_{\rm min}$-soliton at momentum $k_{\rm min} > 0$ with the ground state at $k_{\rm min} < 0$, different dynamics is to be expected: The addition of counter-propagating waves of opposite k will give rise to stripe signatures in the total density. We have numerically solved Eqs. (2), perturbed by the eigenvector $(\mathbf{a}, \mathbf{b})$ of the second anomalous mode, to check this prediction. The bottom panel of Fig. 4 shows the corresponding evolution of the density of the u-component (in which the stripe-forming effect of the perturbation is more evident, since it is the smaller component in our example). Clearly, exciting the second anomalous mode indeed induces a periodic spatial modulation of the background, moving also through the soliton, with a wave number $\sim 2k_{\rm min}$. This modulation effect inside the dark soliton core is reminiscent of the way in which Kelvin modes modulate vortex lines [19].

Lastly, we consider stripe solitons in Regime II [cf. Eq. (15)] in the presence of the trap. The BdG spectrum for such a solution with $\Omega/k_L^2 = 0.625$ is depicted in Fig. 5. As expected from the previous discussion, the spectrum also features two anomalous modes, reflecting the existence of a doubly degenerate lower energy (ground) state. The anomalous modes correspond to an in-phase and an out-of-phase superposition of these ground states, respectively. The former leads to in-phase oscillatory dynamics of the solitons in the two components. This is captured by the lower-lying anomalous mode in the spectrum, as we have checked. On the other hand, the second anomalous mode corresponds to out-of-phase oscillations of the solitons at $k_{\rm min} < 0$ and $k_{\rm min} > 0$. This is directly confirmed by propagation of an initially stationary stripe soliton, perturbed by the respective eigenvector, as shown in the contours of Fig. 6. The dark solitons in each component are shown to perform small-amplitude oscillations; the inset in Fig. 6 depicts the evolution of the center of mass for the individual components, clearly revealing that these are out-of phase oscillations. Additionally, and contrary to $\pm k_{\rm min}$-solitons, Fig. 5 shows that stripe solitons have a small stability domain only close to the linear limit, and become unstable deeper in the nonlinear regime; the instability, though, is found to be induced by the background (*i.e.*, not from the anomalous modes). Apart from subsequent collisions with other modes producing small complex quartets (emerging as small bubbles in the bottom panel of Fig. 5), the two anomalous modes remain purely imaginary, while different background modes generate a cascade of instabilities through the bifurcation of real eigenvalue pairs.

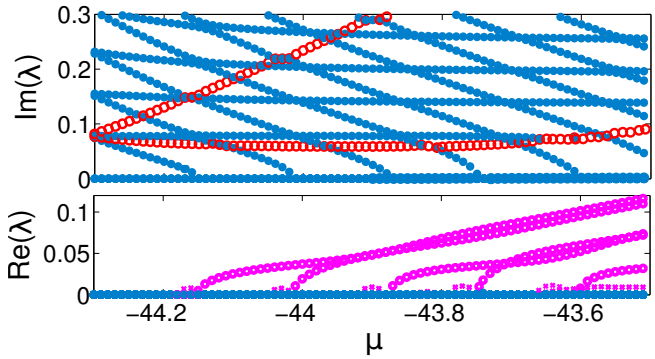

FIG. 5. (Color online) Top and bottom panels show, respectively, the imaginary and real parts of the eigenvalues of the linearization spectrum as functions of μ, for a stripe soliton in Regime II for $\Omega/k_L^2 = 0.625$. The stripe soliton is stable, *i.e.*, $\mathrm{Re}(\lambda) = 0$, only near the linear regime ($\mu \lesssim -44.15$) and becomes unstable deeper in the nonlinear regime. Background instabilities lead to real pairs, while collisions of the anomalous modes with other modes produce weak instabilities via eigenvalue quartets (small bubbles of the bottom panel).

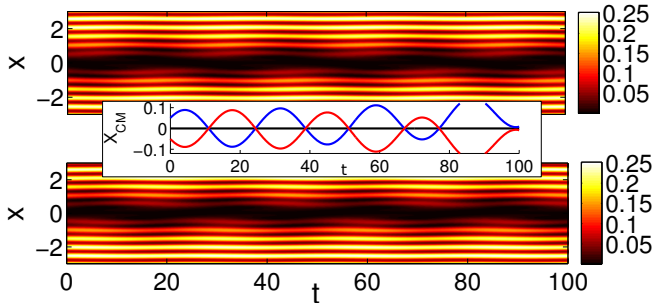

FIG. 6. (Color online) Same as in bottom panel of Fig. 4 but for both components of the stripe soliton in Regime II with $\mu = -44$. The inset middle panel shows the time evolution of the center of mass $x_{\rm cm}$ of the u component (initially at $x_{\rm cm} > 0$ – cf. blue line), of the v component (initially at $x_{\rm cm} < 0$ – cf. red line), and of the total density (black line), at $x_{\rm cm} = 0$.

CONCLUSIONS

In summary, we have studied the existence, stability and dynamics of dark solitons in spin-orbit coupled BECs. We developed a perturbative approach to obtain solitons on top of either constant or spatially modulated background density (stripe solitons). A linear stability analysis has shown that constant background solitons are always stable, while stripe solitons are stable only close to the linear limit. The eigenfrequency of the anomalous mode associated with the oscillatory motion of solitons in a parabolic trap was determined analytically. Importantly, in a certain parameter regime where the single particle spectrum features a double well structure, we found a *second* anomalous mode, which does not exist in single- or multi-component BECs. Exciting this mode, we found that constant background solitons feature a periodic structure of moving stripes in the vicinity of the soliton core, reminiscent of the Kelvin modulation of vortex lines; for stripe solitons, we observed an out-of-phase oscillation of the constituent solitons. Our work paves the way for interesting future studies in spin-orbit coupled BECs, *e.g.*, on (line- or ring-) soliton and vortex stability and dynamics in higher-dimensional settings.

Acknowledgements. We thank P. Engels for helpful comments and NSF, AvH and DFG for financial support.

* jstockho@physnet.uni-hamburg.de

[1] Y.-J. Lin, K. Jimenez-Garcia, and I. B. Spielman, Nature, **471**, 83 (2011).
[2] J.-Y. Zhang, *et al.*, Phys. Rev. Lett. **109**, 115301 (2012).
[3] C. Qu, *et al.*, arXiv:1301.0658.
[4] P. Wang, *et al.*, Phys. Rev. Lett. **109**, 095301 (2012).
[5] L.W. Cheuk, *et al.*, Phys. Rev. Lett. **109**, 095302 (2012).

[6] V. Galitski, and I. B. Spielman, Nature, **494**, 54 (2013).
[7] M. Z. Hasan and C. L. Kane, Rev. Mod. Phys. **82**, 3045 (2010).
[8] J. Dalibard *et al.*, Rev. Mod. Phys. **83**, 1523 (2011).
[9] E. Zohar, J. Cirac, and B. Reznik, Phys. Rev. Lett. **109**, 125302 (2012).
[10] T. L. Ho and S. Zhang, Phys. Rev. Lett. **107**, 150403 (2011); S. Sinha, R. Nath, and L. Santos, Phys. Rev. Lett. **107**, 270401 (2011); Y. Li, L. P. Pitaevskii, and S. Stringari, Phys. Rev. Lett. **108**, 225301 (2012).
[11] Y. Zhang, L. Mao, and C. Zhang, Phys. Rev. Lett. **108**, 035302 (2012); Y. Li, G. Martone, S. Stringari, Europhys. Lett. **99**, 56008 (2012); Z. Chen and H. Zhai, Phys. Rev. A. **86**, 041604 (2012).
[12] T. Kawakami *et al.*, Phys. Rev. Lett. **109**, 015301 (2012); C.-F. Liu and W. M. Liu, Phys. Rev. A **86**, 033602 (2012); X. Zhou, Y. Li, Z. Cai, and C. Wu, arXiv:1301.5403.
[13] X.-Q. Xu and J. H. Han, Phys. Rev. Lett. **107**, 200401 (2011); J. Radić *et al.*, Phys. Rev. A **84**, 063604 (2011); B. Ramachandhran *et al.*, Phys. Rev. A **85**, 023606 (2012).
[14] G. J. Conduit, Phys. Rev. A **86**, 021605(R) (2012).
[15] O. Fialko, J. Brand, and U. Zülicke, Phys. Rev. A **85**, 051605(R) (2012).
[16] V. Achilleos *et al.*, arXiv:1211.0199; Y. Xu, Y. Zhang, and B. Wu, Phys. Rev. A **87**, 013614 (2013).
[17] Y. Kawaguchi and M. Ueda, Phys. Rep. **520**, 253 (2012).
[18] D. J. Frantzeskakis, J. Phys. A **43**, 213001 (2010).
[19] V. Bretin *et al.*, Phys. Rev. Lett. **90**, 100403 (2003); A. L. Fetter, Rev. Mod. Phys. **81**, 647 (2009).
[20] C. T. Kelley, *Solving Nonlinear Equations with Newton's Method* (SIAM, Philadelphia, 2003).